Korea-Australia Rheology Journal, 31(1), 41-47 (February 2019) www.springer.com/13367
DOI: 10.1007/s13367-019-0005-6

Magnetorheological characteristics of carbonyl iron microparticles with different shapes

Jae Yun Lee, Seung Hyuk Kwon and Hyoung Jin Choi*
Department of Polymer Science and Engineering, Inha University, Incheon 22212, Republic of Korea
(Received November 24, 2018; final revision received January 20, 2019; accepted January 22, 2019)

Two different shapes of spherical- and flake-like soft-magnetic carbonyl iron (CI) microparticles were dispersed in silicone oil to prepare magnetorheological (MR) fluids. The magnetic-field dependent rheological behaviors of the MR fluids were scrutinized focusing on their shape effect. Saturation magnetization of the flake-shaped CI was obtained to be slightly lower than that of spherical-shaped CI. However, rheological properties of shear stress, shear viscosity, and storage modulus of the flake-shaped CI MR fluid surpassed those of the spherical-shaped CI MR suspension under applied magnetic field strengths. The flake-shaped CI based MR fluid also demonstrated superior sedimentation stability compared with the spherical-shaped CI. This was due to large surface area, suggesting that the anisotropy of CI particles plays an important role in their MR performance.

Keywords: magnetic particle, carbonyl iron, magnetorheological fluid, sedimentation

1. Introduction

Magnetorheological (MR) materials have drawn significant attention recently because of their status as one of the most attractive actively tunable materials. MR fluids consist of suspensions in which soft-magnetic particles are suspended in non-magnetic mediums such as silicone oil, mineral oil, or aqueous carrier liquid. Depending on the type of suspending media, MR fluids exhibit interesting rheological behaviors with tunable and reversible controllability with a very short response time (within milliseconds) to an applied magnetic field (Ashtiani *et al.*, 2015; de Vicente *et al.*, 2011; Genc and Phulé, 2002). Once the magnetic field is activated to the MR fluids, the initially randomly suspended magnetic particles align quickly with the magnetic field. Hence, a chain-like formation is developed due to interparticle interaction via the magnetic dipole force. In this manner, the magnetic field transforms the MR fluid from a liquid phase to a solid phase. Based on these distinctive characteristics, MR fluids have been applied in a wide range of industrial devices such as MR polishers, dampers, and brakes (Lee *et al.*, 2015; Li *et al.*, 2014; Wang and Liao, 2011; Wang *et al.*, 2013).

Various soft magnetic and ferro-magnetic particles with low magnetic hysteresis (such as magnetite, maghemite, carbonyl iron (CI), *etc.*) have been employed as suspending particles for MR fluids (Ahn *et al.*, 2015; Bica and Anitas, 2018; Gao *et al.*, 2017; Min *et al.*, 2017; Pei *et al.*, 2017; Seo *et al.*, 2016; Tong *et al.*, 2017; Xia *et al.*, 2017; Yang *et al.*, 2017). Among these, CI particles have attracted significant attention because of their low cost, superior magnetism with high saturation magnetization (and no hysteresis), and appropriate size (in the micron order) needed for good MR properties (Genc and Phulé, 2002; Seo *et al.*, 2018). However, severe problems emerge when the CI particles are directly applied in MR fluids. Compared to carrier media, CI particles are heavy. Consequently, they are subjected to rapid sedimentation which causes deteriorated performance of the MR fluids (Ashtiani *et al.*, 2015). To address these issues, several methods have been attempted in the case of spherical-shaped CI particles. For example, surface coating of CI particles and incorporation of additives for better dispersion and improved magnetic property (Kim *et al.*, 2017; Min *et al.*, 2017).

Additionally, the shape of magnetic particle used is known to play an important role with respect to MR properties and dispersion stability. Studies have been carried out investigating the effect of particle shape on MR performance and sedimentation of CI-based MR fluid. Upadhyay *et al.* (2014) investigated sedimentation stability and MR properties in a dynamic mode for spherical- and flake-shaped CI/paraffin liquid based MR fluid. Their study showed that the sedimentation stability of the flake-shaped CI MR fluid was better than that of the spherical-shaped CI MR fluid and the flake-shaped CI MR fluid had higher storage modulus compared with the spherical-shaped CI MR fluid. This was because of the solid friction between the flake-shaped particles depending on the applied magnetic field. However, their report did not address various rheological values such as steady shear stress and shear viscosity for the same grade of CI particles. Recently, Shilan *et al.* (2016) prepared flake-like CI particles from spherical-like CI microspheres through a ball-milling technique. They then compared sedimentation

*Corresponding author; E-mail: hjchoi@inha.ac.kr

stability and rheological behaviors of MR fluid composed of the plate-like CI/polyalphaolefin oil with the spherical-like CI MR fluid. They found the sedimentation stability of the plate-like CI was increased due to increases in frictional forces induced by its large surface area. Also, they determined that yield shear stress of the flake-like CI MR fluid increased up to 270% compared with the spherical-like CI MR fluid (mainly from a steady shear test).

This study aims to compare magnetic properties and sedimentation stabilities of commercial spherical- and flake-like CI particles. Also, magnetic field-dependent viscoelastic behaviors are investigated with respect to particle shape in CI/silicone oil-based MR fluid via steady and dynamic oscillatory tests. Saturation magnetization and sedimentation for the spherical- and flake-shaped CI were measured using a vibrating sample magnetization (VSM) and a Turbiscan, respectively. Steady shear stress and shear viscosity for the MR suspensions (based on the spherical- and flake-shaped CI) were examined via a steady shear test at room temperature with 0-343 kA/m of magnetic field strength. Similarly, a dynamic oscillatory shear test was carried out under the same conditions as the steady shear test to investigate viscoelasticity for the MR fluids. In addition, dynamic yield stress and elastic yield stress were determined from results of the steady and dynamic shear tests. The correlation between yield stresses and saturation magnetization was then considered.

2. Experimental

2.1. Materials and preparation of MR fluids

Both the spherical- and flake-shaped CI particles were purchased from BASF with SQ grade. Their densities were 8.21 and 8.43 g/cm^3, respectively (measured using a pycnometer). The size distribution range of the spherical-shaped CI was about 1-5 μm and that of flake-shaped CI was about 5-50 μm (observed using a microscope). Silicone oil obtained from Shinetsu (Japan) (Kf-96, 100 cS of kinematic viscosity) was used as a medium oil. MR fluids were prepared by suspending the CI particles in the silicone oil with a particle concentration of 50 wt.% (about 10 vol.%) using a vortex mixer (Vortex3, Ika, Germany) and an ultra-sonication bath (Powersonic 401, Hwashin Instrument, Korea). The mixing and sonication times were both 1 h.

2.2. Characterization

A high-resolution scanning electron microscope (HR-SEM) (SU8010, Hitachi, Japan) was used to observe the morphological image of two kinds of CI particles (operated at 15 kV of accelerating voltage). Magnetic characteristics of two types of CI particles were tested using a VSM from −1000 to 1000 kA/m of an applied magnetic field strength at room temperature. In addition, a Turbiscan classic (MA2000, Formulaction Inc., France) was used to compare sedimentation ratios for both types of CI in silicon oil. Characteristics of MR fluids based on spherical- and flake-shaped CI were tested by a torsional rheometer (MCR 300, Anton-Paar, Austria) using a parallel-plate geometry (PP20, 20 mm of diameter) and a magnetic field generator (MRD 180, Anton-Paar, Austria). Under magnetic fields, flow behaviors and viscoelastic properties were determined by steady and dynamic oscillatory shear tests, respectively.

3. Results and Discussion

Figure 1 represents morphological images of the surface of spherical- and flake-shaped CI particles, respectively (observed by SEM). The spherical-shaped CI particles displayed sphere-like morphology having different sizes from approximately 1 to 5 μm. The flake-shaped CI particles showed plate-like morphology with a larger size than that of spherical-shaped CI microspheres. In general, flake-shaped CI particles are produced from spherical-shaped CI microspheres through a ball-milling technique. During the ball-milling process, the CI particles were subjected to welding, fracturing, and re-welding. This resulted in a change of CI particle size (Shilan *et al.*, 2016).

Figure 2 depicts the magnetization-magnetic field strength curve obtained by a VSM. It shows that the saturation magnetization (Ms) values of both spherical- and flake-

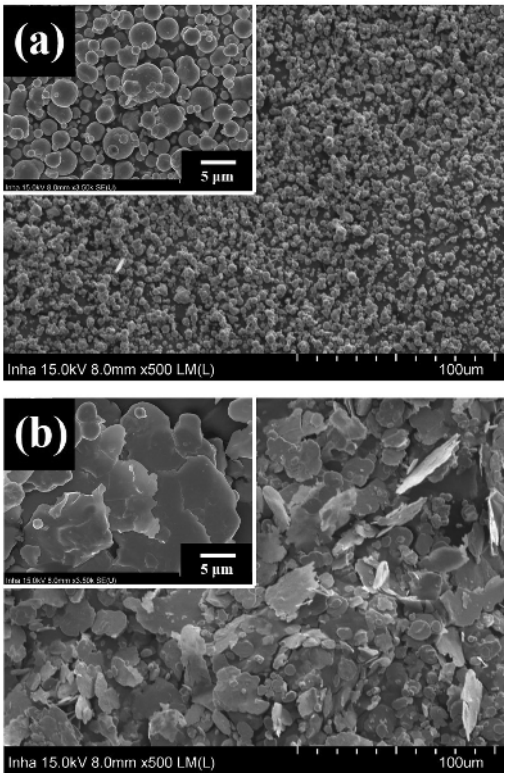

Fig. 1. SEM images for (a) spherical- and (b) flake-shaped CI.

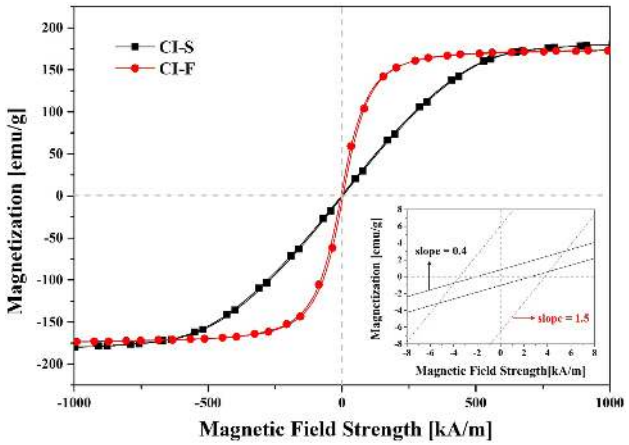

Fig. 2. (Color online) Magnetization-magnetic field strength curve for spherical- (CI-S) and flake-shaped CI (CI-F).

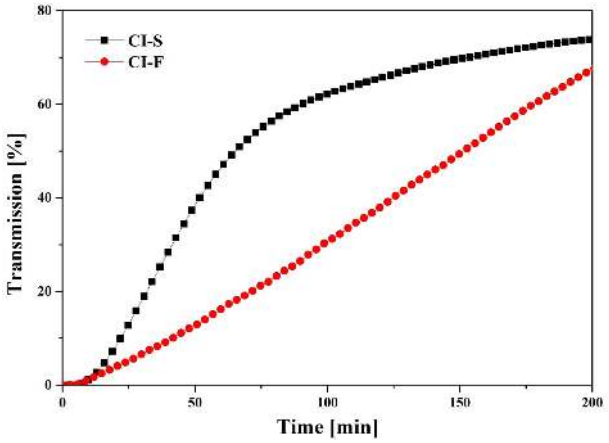

Fig. 3. (Color online) Time-dependent sedimentation ratio for spherical- (CI-S) and flake-shaped CI (CI-F).

shaped CI identified from this curve were approximately 180 and 173 emu/g, respectively. Mass magnetic susceptibilities (obtained from an initial slope of the magnetization-magnetic field strength curve (Cao *et al.*, 2014)) were 0.4×10^{-3} and 1.5×10^{-3} m^3/kg, respectively. Furthermore, the volume magnetic susceptibilities were 3.28 and 12.65 (converted using the density of CI particles). The flake-shaped CI exhibited slightly lower Ms and reached the Ms at a lower magnetic field strength than the spherical-shaped CI. The saturation magnetization of the same magnetic materials could be different depending on size, shape, and oxidation degree of particle (Bell *et al.*, 2007; de Vicente *et al.*, 2010). The flake-shaped CI particles are subjected to an increase of oxidation inside the particles during the ball milling process. Hence, their saturation magnetization might be decreased (Mohamad *et al.*, 2018). Furthermore, the flake-shaped CI represented higher coercive force and residual magnetism than the spherical-shaped CI (as shown in the inset of Fig. 2). The coercive force is affected by shape anisotropy of magnetic particles. Particles with small demagnetization factor should present large coercive force based on the assumption that shape anisotropy is the main mechanism for coercive force (de Vicente *et al.*, 2010). Consequently, it was considered that higher coercive force and residual magnetism could be attributed to achievement of saturation magnetization of the flake-shaped CI at low magnetic field strength.

Figure 3 displays the time-dependent sedimentation stability for spherical- and flake-shaped CI measured using a Turbiscan. The suspension based on the CI particles was prepared by dispersing each of the CI particles in silicone oil with 30 wt.% particle concentration. The sedimentation stability which is directly related to the light transmission from the Turbiscan test was investigated by a following equation:

$$\text{Transmission (\%)} = \frac{\text{Height of light tansmitted through suspension}}{\text{Height of total suspension}} \times 100. \quad (1)$$

The height of light transmitted though the suspension was calculated from the intensity of transmittance light during a sedimentation process of the CI particles. As shown in Fig. 3, it was clearly observed that the flake-shaped CI settled down more slowly in an oil medium than the spherical-shaped CI. This was caused by the high friction force resulting from the large surface area of the flake-shaped CI particles which interfere with sedimentation (Mohamad *et al.*, 2018). On the other hand, it can be also noted that a shape correction factor has been recently implied for its effect on sedimentation (Son, 2018).

Figure 4 represents shear rate dependent both (a) shear stress and (b) shear viscosity on a log-log scale for MR fluids based on both spherical- and flake-shaped CI under external magnetic fields. Without the applied magnetic field, both MR fluids indicated that shear stress at a low shear rate was close to zero but gradually increased with an increased shear rate (demonstrating a fluid-like property). In the absence of the magnetic field, shear viscosity of various typical magnetic suspensions has drawn huge attention regarding various experimental conditions (Jeon and Koo, 2012). With applied magnetic fields, shear stress of both MR suspensions was increased significantly in a low shear rate region and became stable over the whole shear rate. This indicates that the shear stress behavior of both MR fluids is solid-like. This tendency resulted from the chain-like organization induced by magnetic dipole interactive force between adjacent particles in the presence of magnetic fields (Zhang and Widom, 1995). Additionally, the shear stress grew with an applied magnetic field intensity. The shear stress of the flake-shaped CI MR fluid became larger than that of the spherical-shaped CI

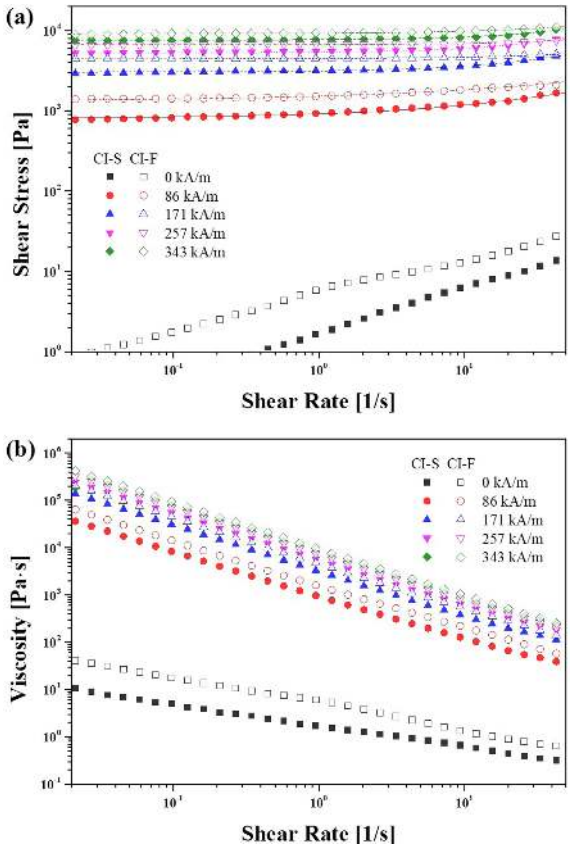

Fig. 4. (Color online) Magnetic field-dependent flow curve for spherical- (CI-S, closed symbol) and flake-shaped CI MR fluids (CI-F, open symbol): (a) Shear stress and (b) viscosity.

MR suspension. This is considered to be due to the large contact surface of the flake-shaped CI particles allowing the formation of sturdy clusters under the applied magnetic field and because the solid friction among them was increased (Shilan *et al.*, 2016).

The Bingham fluid model is suitable for fitting flow curves for typical MR fluids possessing yield stress resulting from chain-like formation of magnetic particles. It was used here to fit the flow curve of the MR fluids as follows (Park *et al.*, 2011):

$$\tau = \tau_0 + \eta_0 \dot{\gamma}, \quad \tau \geq \tau_0 ,$$
$$\dot{\gamma} = 0, \quad \tau < \tau_0 \tag{2}$$

where τ_0, η_0, and $\dot{\gamma}$ are defined as yield stress, shear viscosity, and shear rate, respectively. As presented in Fig. 4a, both solid-line and dashed line indicate the stress curve of spherical- and flake-shaped CI based MR fluids, respectively. These were obtained using a Bingham model, which agreed well with the experimental data of both MR fluids.

The shear viscosity of both MR suspensions was very low (~10-10^2 Pa·s) at the low shear rate regime without an applied magnetic field, but it increased gradually with increased magnetic field strength (as shown in Fig. 4b). Both MR fluids also presented shear-thinning property and decrease of shear viscosity with a shear rate over the whole shear rate. The shear viscosity of the flake-shaped CI MR suspension surpassed that of the spherical-shaped CI MR suspension (similar to the shear stress behaviors).

To further investigate the viscoelasticity of both MR fluids under applied magnetic fields, dynamic oscillatory shear tests were carried out over a range of magnetic field

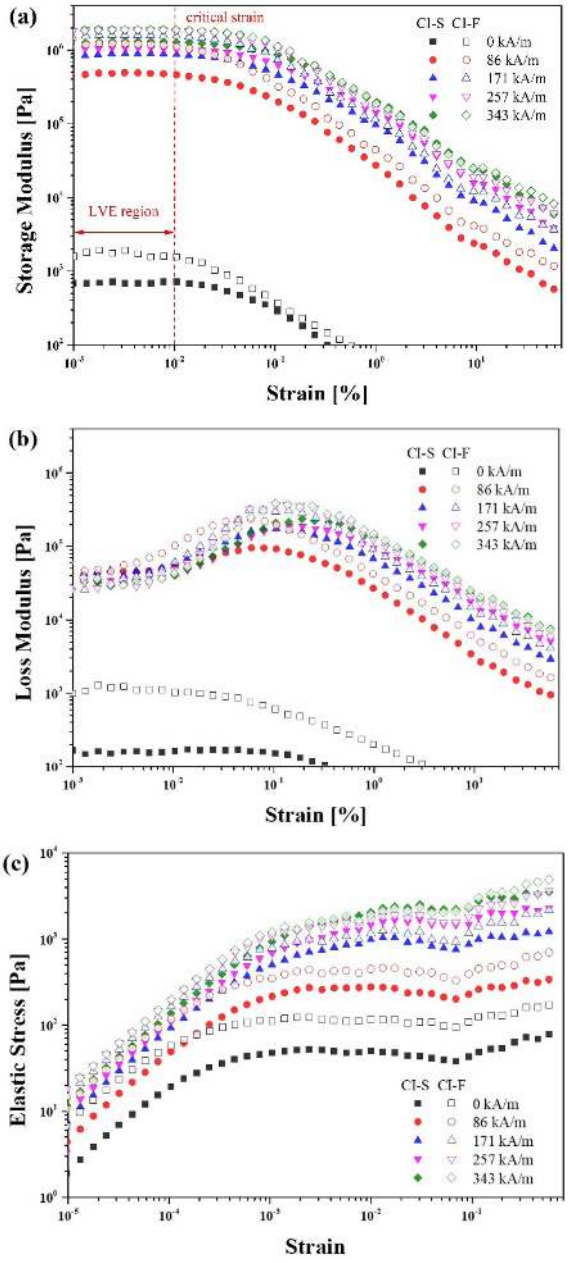

Fig. 5. (Color online) The results of amplitude sweep test depending on magnetic field for spherical- (CI-S, closed symbol) and flake-shaped CI MR fluids (CI-F, open symbol): (a) Storage modulus, (b) loss modulus, and (c) elastic yield stress.

strengths (0-343 kA/m). Figure 5 depicts both (a) storage and (b) loss moduli for both MR fluids as a function of strain. The strain is measured via an amplitude sweep test performed at a constant frequency (6.28 rad/s) over a strain range of 1×10^{-3} to 7×10%. Both MR fluids showed a low storage modulus in low strain regions without the applied magnetic field. With a magnetic field applied to both MR fluids, their storage moduli steadily increased with increased magnetic field strength. A plateau region then followed, a so-called linear viscoelastic (LVE) region. The storage moduli decreased gradually as it passed a critical strain due to a deformed state change from a solid-like to a liquid-like phase (Claracq *et al.*, 2004; Fang *et al.*, 2008; Peng *et al.*, 2014). Consequently, the constant strain for a further frequency sweep test was selected to be 0.005% via the amplitude sweep test. To study the yielding behavior from the dynamic oscillatory shear experiment, the in-phase stress value (so called elastic stress) was plotted using the storage moduli, as given in Fig. 5c. The elastic stress in the LVE region was found to increase linearly with increasing strain.

Figure 6 shows (a) storage and (b) loss moduli for both MR fluids as function of angular frequency obtained through an angular frequency sweep test performed with 0.005% of strain over a frequency range of 2-200 rad/s. As shown in Fig. 6a, both MR fluids (without the applied magnetic field) revealed a liquid-like behavior with continuously increasing storage modulus from a low to a high angular frequency area. However, on applying the magnetic field both MR suspensions exhibited a solid-like behavior with dramatically increased storage modulus at a low angular frequency regime. This was followed by a plateau region over the whole angular frequency range. As mentioned above, the magnetic particles aligned with a chain-like form with external magnetic fields. This resulted in the increased storage moduli. Furthermore, the storage moduli were increased further and further with increased magnetic field intensity. The storage moduli of the flake-shaped CI MR fluid were superior to those of spherical-shaped CI MR fluid.

On the other hand, Schwarzl equation calculates stress relaxation modulus from storage and loss modulus in the frequency sweep test. It can be used in the identification of solid-like behavior as follows (Emri *et al.*, 2005):

$$G(t)\approx G'(\omega)-0.566G''(\omega/2)+0.203G''(\omega)\,. \tag{3}$$

Figure 7 depicts the variation of time-dependent shear relaxation moduli of both MR suspensions with or without the magnetic field according to Eq. (3). Without the magnetic field, the relaxation moduli of both MR suspensions decreased with time. Under applied magnetic fields, the relaxation moduli became almost constant regardless of the time because of strong interaction between adjacent particles. This clearly indicated a solid-like behavior.

Furthermore, the dynamic (τ_y) and elastic ($G'\gamma$) yield stresses for both MR fluids were plotted as a function of magnetical field strength as shown in Fig. 8. Both τ_y and $G'\gamma$ were determined by the shear stress at zero shear rate limit on the flow curve and yield point on elastic stress-strain curve, respectively. Generally, the τ_y in the MR fluid is increased with increasing magnetic field intensity. The

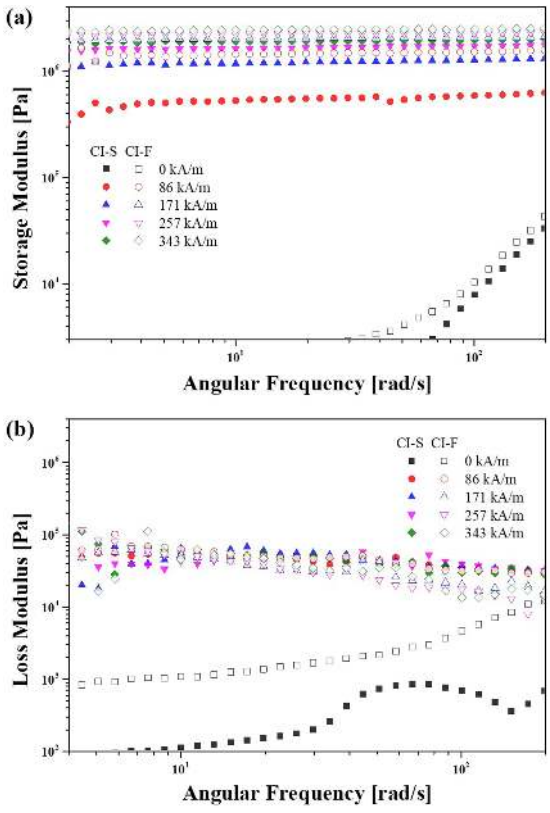

Fig. 6. (Color online) The results of angular frequency sweep test depending on magnetic field for spherical- (CI-S, closed symbol) and flake-shaped CI MR fluids (CI-F, open symbol): (a) Storage modulus and (b) loss modulus.

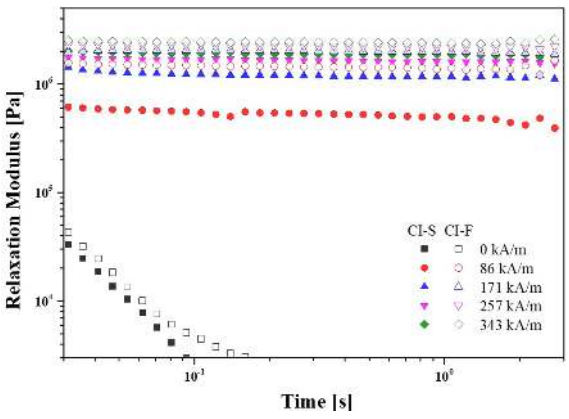

Fig. 7. (Color online) Time-dependent relaxation modulus for spherical- (CI-S, closed symbol) and flake-shaped CI MR fluids (CI-F, open symbol).

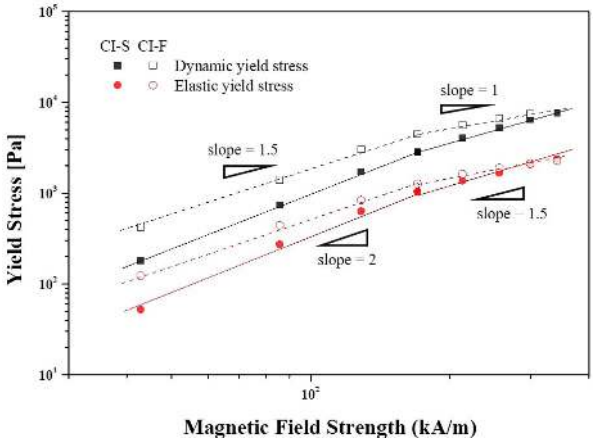

Fig. 8. (Color online) Dynamic- and elastic yield stress as function of magnetic field strength for spherical- (CI-S, closed symbol) and flake-shaped CI MR fluids (CI-F, open symbol).

correlation between τ_y and magnetic field strength is as follows (Genc and Phulé, 2002):

$$\tau_y \propto H^{\alpha}. \tag{4}$$

In a low magnetic field region, α is commonly 2 according to the polarization model relevant to the mutual attraction between magnetic particles due to polarization force (Fang *et al.*, 2011). However, since the localized saturation magnetization is usually increased while the magnetization of MR fluid being fully the saturation with increasing magnetic field strength, the magnetic polarization force between soft magnetic particles decreases in the intermediate range of magnetic field strength and α becomes smaller than 2. Therefore, the local saturation is of considerable importance. τ_y is described as follows (Ginder *et al.*, 1996):

$$\tau_y = \sqrt{6}\phi\mu_0 M_s^{1/2} H^{3/2} \tag{5}$$

where ϕ, μ_0, and M_s are defined as the particle volume fraction in MR fluid, the permeability of free space, and the maximum value at the MR fluid's local saturation magnetization. Provided that the magnetization of MR fluid reaches full saturation at high magnetic field strength, yield stress is hardly affected by the magnetic field. This shows the independent relationship to be as follows (Ginder *et al.*, 1996):

$$\tau_y^{sat} = 0.086\phi\mu_0 M_s^2. \tag{6}$$

α could be changed by applying a critical magnetic field strength (H_c), where it is 2 in the region below H_c but 1.5 in the region above H_c. As presented in Fig. 6, spherical-shaped CI based MR suspension indicated that τ_y and $G'\gamma$ initially increased in proportion to H^2 and then increased in proportion to $H^{1.5}$ when the magnetic field strength surpassed 171 kA/m. For the flake-shaped CI MR fluid, τ_y and $G'\gamma$ increased in proportion to $H^{1.5}$ over the magnetical field strength range of 43 to 171 kA/m and then increased in proportion to H^1 when the magnetical field strength exceeded 171 kA/m. For the VSM result, it was assumed that the magnetization of the flake-shaped CI based MR fluid was already locally saturated at extremely low magnetic field strength and was fully saturated at 171 kA/m.

4. Conclusions

The morphology, saturation magnetization, and sedimentation rate for two different shaped CI particles (spherical- and flake-shape) of the same commercial-grade were examined. The magnetic field-dependent rheological characteristics for MR fluid based on both CIs were compared. It was observed using SEM that the particle size of the flake-shaped CI was larger than that of the spherical-shaped CI. This size difference was due to the production process of the flake-shaped CI which included welding, fracturing, and re-welding. In the magnetization-magnetic field strength curve, the saturation magnetization of flake-shaped CI (~173 emu/g) was lower than spherical-shaped CI (~180 emu/g) because of an increase of oxidation inside the particles. However, the sedimentation stability of the flake-shaped CI was superior to that of the spherical-shaped CI due to high friction force.

Two types of MR fluid were prepared by dispersing each of the different shaped CIs in silicone oil at 50 wt.%. Magnetic-field dependent rheological characteristics were measured using steady and dynamic shear tests. Under the applied magnetic field, shear stress and storage modulus measurements of the flake-shaped CI MR fluid surpassed those of the spherical-shaped CI MR fluid. This was considered to be due to a construction of sturdy clusters and an increase of solid friction. In addition, dynamic and elastic yield stress measurements were plotted to gain insight into the saturation magnetization in terms of rheology. These plots indicated the local saturation magnetization of the spherical-shaped CI MR fluid and the complete saturation magnetization of the flake-shaped CI MR fluid at 171 kA/m of magnetic field strength.

Acknowledgements

This work was supported by National Research Foundation of Korea (2018R1A4A1025169).

References

Ahn, W.J., H.S. Jung, and H.J. Choi, 2015, Pickering emulsion polymerized smart magnetic poly(methyl methacrylate)/Fe_2O_3 composite particles and their stimulus-response, *RSC Adv.* **5**, 23094-23100.

Ashtiani, M., S.H. Hashemabadi, and A. Ghaffari, 2015, A review on the magnetorheological fluid preparation and stabilization,

J. Magn. Magn. Mater. **374**, 716-730.
Bell, R.C., E.D. Miller, J.O. Karli, A.N. Vavreck, and D.T. Zimmerman, 2007, Influence of particle shape on the properties of magnetorheological fluids, *Int. J. Mod. Phys. B* **21**, 5018-5025.
Bica, I. and E.M. Anitas, 2018, Magnetic field intensity effect on electrical conductivity of magnetorheological biosuspensions based on honey, turmeric and carbonyl iron, *J. Ind. Eng. Chem.* **64**, 276-283.
Cao, Q., X. Han, and L. Li, 2014, Configurations and control of magnetic fields for manipulating magnetic particles in microfluidic applications: Magnet systems and manipulation mechanisms, *Lab Chip* **14**, 2762-2777.
Claracq, J., J. Sarrazin, and J.P. Montfort, 2004, Viscoelastic properties of magnetorheological fluids, *Rheol. Acta* **43**, 38-49.
de Vicente, J., D.J. Klingenberg, and R. Hidalgo-Alvarez, 2011, Magnetorheological fluids: A review, *Soft Matter* **7**, 3701-3710.
de Vicente, J., F. Vereda, J.P. Segovia-Gutiérrez, M. del Puerto Morales, and R. Hidalgo-Álvarez, 2010, Effect of particle shape in magnetorheology, *J. Rheol.* **54**, 1337-1362.
Emri, I., B.S. von Bernstorff, R. Cvelbar, and A. Nikonov, 2005, Re-examination of the approximate methods for interconversion between frequency- and time-dependent material functions, *J. Non-Newton. Fluid Mech.* **129**, 75-84.
Fang, F.F., M.S. Yang, and H.J. Choi, 2008, Novel magnetic composite particles of carbonyl iron embedded in polystyrene and their magnetorheological characteristics, *IEEE Trans. Magn.* **44**, 4533-4536.
Fang, F.F., Y.D. Liu, H.J. Choi, and Y. Seo, 2011, Core-shell structured carbonyl iron microspheres prepared via dual-step functionality coatings and their magnetorheological response, *ACS Appl. Mater. Interfaces* **3**, 3487-3495.
Gao, C.Y., M.W. Kim, D.H. Bae, Y.Z. Dong, S.H. Piao, and H.J. Choi, 2017, Fe_3O_4 nanoparticle-embedded polystyrene composite particles fabricated via a Shirasu porous glass membrane technique and their magnetorheology, *Polymer* **125**, 21-29.
Genc, S. and P.P. Phulé, 2002, Rheological properties of magnetorheological fluids, *Smart Mater. Struct.* **11**, 140-146.
Ginder, J.M., L.C. Davis, and L.D. Elie, 1996, Rheology of magnetorheological fluids: Models and measurements, *Int. J. Mod. Phys. B* **10**, 3293-3303.
Jeon, J. and S. Koo, 2012, Viscosity and dispersion state of magnetic suspensions, *J. Magn. Magn. Mater.* **324**, 424-429.
Kim, M.H., K. Choi, J.D. Nam, and H.J. Choi, 2017, Enhanced magnetorheological response of magnetic chromium dioxide nanoparticle added carbonyl iron suspension, *Smart Mater. Struct.* **26**, 095006.
Lee, J.W., K.P. Hong, M.W. Cho, S.H. Kwon, and H.J. Choi, 2015, Polishing characteristics of optical glass using PMMA-coated carbonyl-iron-based magnetorheological fluid, *Smart Mater. Struct.* **24**, 065002.
Li, Y., J. Li, W. Li, and H. Du, 2014, A state-of-the-art review on magnetorheological elastomer devices, *Smart Mater. Struct.* **23**, 123001.
Min, T.H., H.J. Choi, N.H. Kim, K. Park, and C.Y. You, 2017, Effects of surface treatment on magnetic carbonyl iron/polyaniline microspheres and their magnetorheological study, *Colloid Surf. A-Physicochem. Eng. Asp.* **531**, 48-55.
Mohamad, N., Ubaidillah, S.A. Mazlan, F. Imaduddin, S.B. Choi, and I.I.M. Yazid, 2018, A comparative work on the magnetic field-dependent properties of plate-like and spherical iron particle-based magnetorheological grease, *PLoS One* **13**, e0191795.
Park, B.O., B.J. Park, M.J. Hato, and H.J. Choi, 2011, Soft magnetic carbonyl iron microsphere dispersed in grease and its rheological characteristics under magnetic field, *Colloid Polym. Sci.* **289**, 381-386.
Pei, L., H. Pang, X. Ruan, X. Gong, and S. Xuan, 2017, Magnetorheology of a magnetic fluid based on Fe_3O_4 immobilized SiO_2 core-shell nanospheres: Experiments and molecular dynamics simulations, *RSC Adv.* **7**, 8142-8150.
Peng, G.R., W. Li, T.F. Tian, J. Ding, and M. Nakano, 2014, Experimental and modeling study of viscoelastic behaviors of magneto-rheological shear thickening fluids, *Korea-Aust. Rheol. J.* **26**, 149-158.
Seo, Y.P., S. Han, J. Choi, A. Takahara, H.J. Choi, and Y. Seo, 2018, Searching for a stable high-performance magnetorheological suspension, *Adv. Mater.* **30**, 1704769.
Seo, Y.P., S. Kwak, H.J. Choi, and Y. Seo, 2016, Static yield stress of a magnetorheological fluid containing Pickering emulsion polymerized Fe_2O_3/polystyrene composite particles, *J. Colloid Interface Sci.* **463**, 272-278.
Shilan, S.T., S.A. Mazlan, Y. Ido, A. Hajalilou, B. Jeyadevan, S.B. Choi, and N.A. Yunus, 2016, A comparison of field-dependent rheological properties between spherical and plate-like carbonyl iron particles-based magneto-rheological fluids, *Smart Mater. Struct.* **25**, 095025.
Son, K.J., 2018, A discrete element model for the influence of surfactants on sedimentation characteristics of magnetorheological fluids, *Korea-Aust. Rheol. J.* **30**, 29-39.
Tong, Y., X. Dong, and M. Qi, 2017, High performance magnetorheological fluids with flower-like cobalt particles, *Smart Mater. Struct.* **26**, 025023.
Upadhyay, R.V., Z. Laherisheth, and K. Shah, 2014, Rheological properties of soft magnetic flake shaped iron particle based magnetorheological fluid in dynamic mode, *Smart Mater. Struct.* **23**, 015002.
Wang, D.H. and W.H. Liao, 2011, Magnetorheological fluid dampers: A review of parametric modelling, *Smart Mater. Struct.* **20**, 023001.
Wang, D.M., Y.F. Hou, and Z.Z. Tian, 2013, A novel high-torque magnetorheological brake with a water cooling method for heat dissipation, *Smart Mater. Struct.* **22**, 025019.
Xia, Z., X. Wu, G. Peng, L. Wang, W. Li, and W. Wen, 2017, A novel nickel nanowire based magnetorheological material, *Smart Mater. Struct.* **26**, 054006.
Yang, J., H. Yan, J. Dai, Z. Hu, and H. Zhang, 2017, The rheological response of carbonyl iron particles suspended in mineral oil solution of 12-hydroxy stearic acid, *J. Rheol.* **61**, 515-524.
Zhang, H. and M. Widom, 1995, Field-induced forces in colloidal particle chains, *Phys. Rev. E* **51**, 2099-2103.